Layer-by-Layer Assembled Polyaniline Nanofiber/Multiwall Carbon Nanotube Thin Film Electrodes for High-Power and High-Energy Storage Applications

Md Nasim Hyder,[†,∥] Seung Woo Lee,[†,⊥,∥] Fevzi Ç. Cebeci,[†,#] Daniel J. Schmidt,[†] Yang Shao-Horn,[‡,§,⊥,*] and Paula T. Hammond[†,*]

[†]Department of Chemical Engineering, [‡]Department of Mechanical Engineering, [§]Department of Materials Science and Engineering, and [⊥]Electrochemical Energy Laboratory, Massachusetts Institute of Technology, Cambridge, Massachusetts 02139, United States. [∥]These authors contributed equally to this work. [#]Present address: Sabanci University, Tuzla, Istanbul, Turkey.

ABSTRACT Thin film electrodes of polyaniline (PANi) nanofibers and functionalized multiwall carbon nanotubes (MWNTs) are created by layer-by-layer (LbL) assembly for microbatteries or -electrochemical capacitors. Highly stable cationic PANi nanofibers, synthesized from the rapid aqueous phase polymerization of aniline, are assembled with carboxylic acid functionalized MWNT into LbL films. The pH-dependent surface charge of PANi nanofibers and MWNTs allows the system to behave like weak polyelectrolytes with controllable LbL film thickness and morphology by varying the number of bilayers. The LbL-PANi/MWNT films consist of a nanoscale interpenetrating network structure with well developed nanopores that yield excellent electrochemical performance for energy storage applications. These LbL-PANi/MWNT films in lithium cell can store high volumetric capacitance (~238 ± 32 F/cm^3) and high volumetric capacity (~210 mAh/cm^3). In addition, rate-dependent galvanostatic tests show LbL-PANi/MWNT films can deliver both high power and high energy density (~220 Wh/L$_{electrode}$ at ~100 kW/L$_{electrode}$) and could be promising positive electrode materials for thin film microbatteries or electrochemical capacitors.

KEYWORDS: polyaniline · carbon nanotubes · layer-by-layer assembly · nanostructured electrodes · lithium-ion batteries · electrochemical capacitors

The trend of being lightweight and the small form factor of portable electronic devices strongly requires the development of microscale energy sources having high power, high energy, and a long cycle life. Thin film microbatteries[1] and electrochemical capacitors (ECs)[2] are the most promising energy sources that can meet these demands. Recent advancement of nanostructured electrodes[2−7] has significantly increased performance of thin-film batteries or ECs, but further application for quickly evolving electronic devices will demand both high power density and high energy density within confined volume or footprint areas.

A conjugated polymer, polyaniline (PANi), has been considered a promising battery and EC material because of its high conductivity, thermal and environmental stability, and interesting redox behavior.[8−13] Because of the existence of redox states in the presence of dopants, the intrinsic electron-conducting PANi has demonstrated high electrochemical capacitance over 400 F/g.[11−13] Over the past two decades, several novel methodologies have been developed for the preparation of nanostructured PANi in the form of dispersions, nanowires, nanofibers, and nanotubules that have found applications in rechargeable batteries, microelectronics, sensors, electrochromic displays, and light-emitting and photovoltaic devices.[9−13]

Incorporation of carbon nanotubes (CNTs)[14−16] into an electrochemically active polymer system improves the electrical conductivity as well as the mechanical properties of the original polymer films.[11,12] Since the redox reactions are localized to the thin surface layer of PANi, depositing nanoscale PANi on CNT-based highly porous support films would be an ideal electrode structure for electrochemical energy storage applications. In recent years, significant research efforts have been made to fabricate nanostructured PANi/CNT composites using various approaches from electropolymerization to interfacial polymerization using template-directed or template-free approaches.[11−13,17−19] All of these approaches require some form of pre or post treatment of samples such as removal of templates, separation of solvents, or special experimental conditions that are often not straightforward.

A versatile, straightforward method for fabrication of nanostructured films with controlled compositions is layer-by-layer (LbL) assembly.[20] The LbL technique consists of repeated, sequential immersion of a

* Address correspondence to shaohorn@mit.edu, hammond@mit.edu.

Received for review May 19, 2011 and accepted October 7, 2011.

Published online October 07, 2011
10.1021/nn2029617

© 2011 American Chemical Society

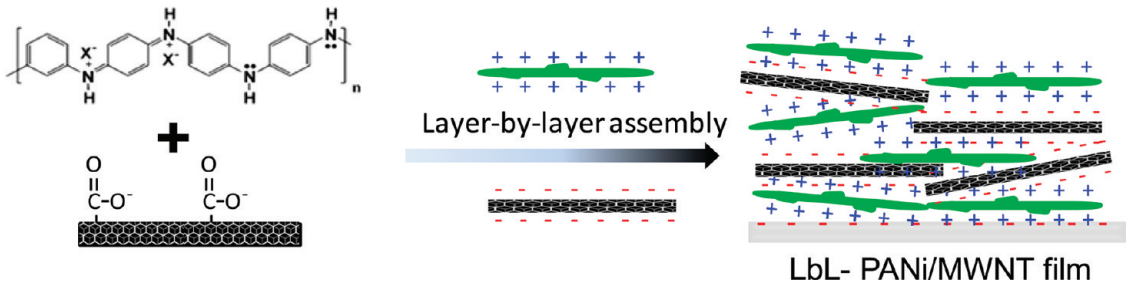

Scheme 1. Layer-by-Layer (LbL) Assembled PANi/MWNT (LbL-PANi/MWNT) Thin Film with Positively Charged PANI Nanofibers and Negatively Charged MWNTs

substrate into aqueous solutions of complementarily functionalized materials and can be employed for a wide diversity of materials where the conformal ultrathin film fabrication is performed under mild conditions on various substrates.[20−22] Recently, we demonstrated that electrostatic LbL assembly can be used to generate all-multiwall carbon nanotube (MWNT) thin films with controlled morphologies and nanoporosity. The resulting films yielded unique positive electrodes for lithium-ion batteries that exhibit high power and high energy density due to the combination of chemical redox reactions and high surface area capacitive storage. In general, functionalized CNTs and CNT composites with conjugated polymers have been of interest for various energy storage and conversion devices shown to exhibit improved networks for electrochemical energy applications.[23,24]

This work describes the fabrication and characterization of ultrathin conformal film electrodes of PANi nanofibers and carboxylic acid functionalized MWNT using the LbL method. For the synthesis of positively charged PANi nanofibers, rapid polymerization in protonic (HCl) media was used, which is a new and powerful approach for the production of comparatively large amounts of water-dispersible PANi fibers.[9] The resulting PANi nanofibers have a net positive charge due to their inherent structure, whereas oxidative treatments yielded negatively charged MWNTs with carboxylic acid groups.[23,25] PANi fibers and acid functionalized MWNTs can be treated much like weak polyelectrolytes (PE) that can be readily used for the LbL method (Scheme 1). Compared to other multilayer assemblies, our approach incorporate irregularly shaped PANi nanofibers and tubular MWNT that enables the direct formation of a porous nanostructure with high surface area. The as-prepared PANi/MWNT film thicknesses show superlinear growth as a function of the number of bilayers. To improve the mechanical stability, the LbL films were heat-treated to control interdiffusion and improve electrical conductivity. Here we address the composition of these fiber/CNT systems, the internal morphology of PANi/MWNT thin films, and the impact on final properties. Electrochemical tests in lithium cells show that these LbL-PANi/MWNTL films can deliver both high power and high energy density (~220 Wh/$L_{electrode}$ at ~100 kW/$L_{electrode}$), making them promising electrode materials for positive electrodes of thin-film microbatteries or ECs. Moreover, we show that utilization of Faradaic reactions between PANi fibers and PF_6^- anions and between oxygen surface functional groups on MWNTs and lithium ions within the 3-dimensional porous network structure are responsible for the high performance.

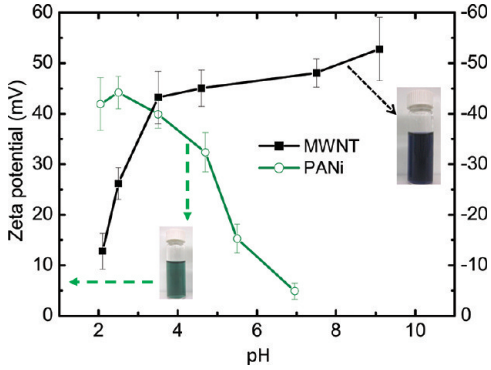

Figure 1. pH-dependent zeta potential of PANi nanofibers and MWNTs. Each point of zeta potential value was obtained by more than 4 measurements, and error bars show standard deviations.

RESULTS AND DISCUSSION

PANi nanofibers were incorporated into an electrostatic LbL system as a positively charged polyelectrolyte with a carboxylated MWNT[23] as the complementary negatively charged polyelectrolyte on ITO-coated glass substrates. Polyaniline emeraldine base, in the presence of a protonic acid such as HCl (1 M) that provides necessary counterions, exists as the emeraldine salt where the imine nitrogens are protonated, yielding positively charged PANi nanofibers suspension. Carboxylic acid groups (-COOH) on the surface of MWNTs exist as carboxylate anions (COO^-) in aqueous solution, yielding negatively charged MWNTs (MWNT-COO^-), for the buildup of LbL films. By simply controlling the number of dipping cycles (the number of bilayers), we precisely assemble LbL-PANi/MWNT films on the substrate with thicknesses in the range of 0.1−1.6 μm. To improve the mechanical stability and electrical conductivity, LbL-PANi/MWNT films were heat-treated at 180 °C for 12 h under vacuum.

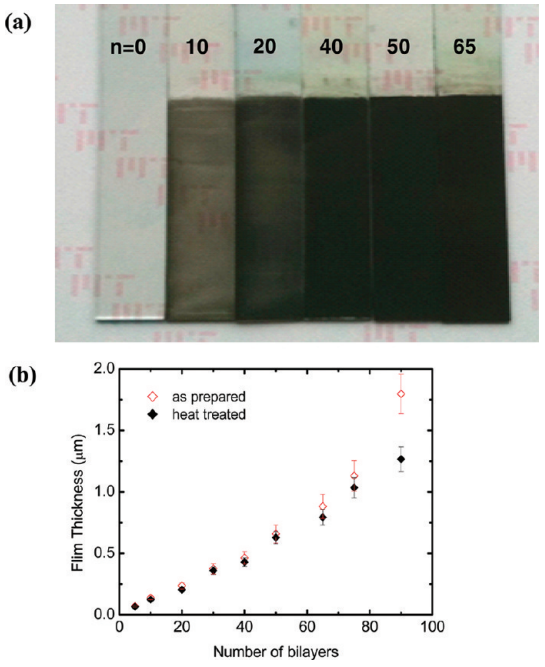

Figure 2. (a) Representative digital picture image of assembled LbL-PANi/MWNT thin films on ITO-coated glass slides. Number on image indicates the number of bilayers (n) in $(PANi/MWNT)_n$. (b) Thickness of the thin films as a function of the number of bilayers: open diamond (red) with standard deviations as error bars for as-prepared films, filled diamond (black) for the heat-treated films. pH 2.5 (+)/3.5 (−) indicates PANi/MWNT thin films assembled from PANi at pH 2.5 and MWNT at pH 3.5.

LbL Assembly of PANi/MWNT Films. To achieve conformal LbL assembled films, it is necessary to determine the optimal surface charges of PANi fibers and MWNT for stable colloidal dispersions. As shown in Figure 1, the zeta potential of the PANi decreased as the pH was increased as a result of changes in the degree of ionization of the amine or imine group on the PANi nanofibers, and the zeta potential of MWNT-COOH was found to decrease with decreasing pH as a result of the protonation of the COOH group on the MWNTs, which is very similar to weak polyelectrolytes such as poly(allylamine hydrochloride) (PAH) and poly(acrylic acid) (PAA).[23,26]

In this study, the cationic nature of partially doped PANi (at pH∼2.5) was chosen to build up multilayer assembly *via* the electrostatic attractions developed with the polyanion of MWNT (at pH ∼3.5). The thickness and morphology of the resulting LbL films can be controlled in a manner similar to weak polyelectrolytes by altering the assembly pH values.[23] It should be noted that the PANi dispersions were not stable below pH 2 and above pH 7; at these conditions, polymer would precipitate within a few hours of preparation, so such conditions could not be used to build up LbL multilayer films.

Figure 2a shows representative optical images of the heat-treated PANi/MWNT thin films on ITO-coated glass slides for different number of bilayers. The LbL films appear darker with increasing number of bilayers due to the adsorbed MWNT that were highly conformal and uniform. In Figure 2b, the thickness of PANi/MWNT LbL films before and after heat treatment is demonstrated, as a function of the number of bilayers. Interestingly, a super linear growth of the thickness was observed with the number of bilayers.

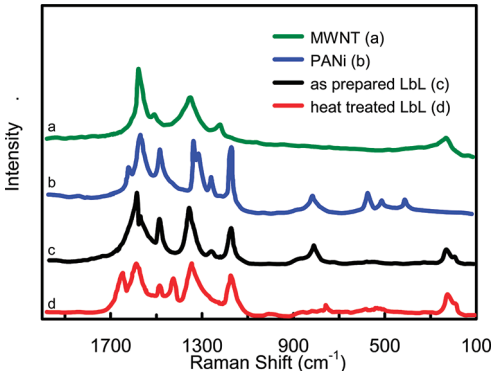

Figure 3. Raman spectra of the LbL-PANi/MWNT films before and after heat treatment. PANi (b) and MWNT (a) are shown as control.

Typically polyelectrolyte (PE) thin films exhibit linear thickness growth with increasing bilayers.[26] Certain LbL systems have been observed to exhibit superlinear film growth in dipped LbL films due to a process of polyelectrolyte interdiffusion within the film.[27,28] In some cases, such as partially charged weak PEs, films actually exhibit an exponential thickness growth regime. This growth could be due to the interdiffusion of polyelectrolyte into and out of the film and to the roughness of the PANi nanofibers and MWNTs that may lead to nanostructures with random properties that are not desirable.[29] There is a growing interest in controlling and understanding the interdiffusion in polyelectrolyte system by adjusting pH or heat treatment.[25,26] The as-prepared PANi/MWNT films were heat-treated at 180 °C for 12 h under vacuum to improve the stability of the films. Any LbL-PANi/MWNT films over 30 bilayers were heat-treated more than once to control the interdiffusion, *e.g.*, LbL-$(PANi/MWNT)_{50}$ film was heat-treated twice, once after the first 30 bilayers and then after the 50th bilayer during LbL assembly. It can be seen that the thickness of the heat-treated PANi/MWNT films show a linear growth behavior with the number of bilayers that are typical of polyelectrolyte bilayers.[26]

Composition and Surface Chemistry of LbL-PANi/MWNT Films. In Supporting Information, Figure S1, the thermogravimetric scans of the LbL films are shown before and after heat treatment along with PANi nanofibers and MWNT as control. The weight of the sample has been recorded as a function of temperature from 30 to 850 °C. The HCl doped PANi nanofibers show a gradual decomposition process: initially between 100 and 200 °C due to the

volatilization of water molecules, dopants, and oligomers or any unreacted monomer elimination; between 200 and 550 °C due to the elimination of dopant HCl and decomposition of main chain of PANi; and finally, at higher temperatures between 600 and 850 °C, the polymer backbone chain breakage can lead to production of gases such as acetylene and ammonia.[31] On the other hand, the MWNT sample shows initial weight loss from 100 to 300 °C due to the organic decomposition of carboxylic acid from the side walls of MWNTs, and the weight loss from 450 to 680 °C is attributed to the oxidation of MWNTs. For the heat-treated LbL film, the TGA thermogram shows similar behavior as PANi where the weight loss starts at 200 °C, which corresponds to the decomposition of polymer; continues between 500 and 700 °C, which corresponds to oxidation of MWNTs; and shows a residual weight of 23% which could be due to the presence of impurities in the MWNTs. It is interesting to note that compared to the heat-treated LbL film, the as-prepared LbL film starts losing water around 80 °C and loses about 6% weight before reaching 200 °C. The relative compositions of PANi and MWNT in the LbL films were determined from the derivative of weight loss/temperature using the decomposition of PANi and MWNT (shown in Supporting Information, Figure S1b) as control measurements.[30] For 65 bL of LbL-PANi/MWNT film, a composition of 57 ± 8 wt % PANi and 43 ± 5 wt % of MWNT was observed.

The density (global average) of LbL-PANi/MWNT thin films was obtained by calculating the deposited mass of the LbL films with a quartz crystal microbalance QCM (Masscal G1, Florida) (Supporting Information, Figure S2). By obtaining the film thickness and active area of the quartz crystal on which the LbL film was deposited, the mass was then calculated using the Sauerbray equation.[32] The mass average density was then calculated from the buildup volume of the LbL-PANi/MWNT film before and after heat treatment, 0.64 and 0.57 g/cm^3, respectively. This result is in good agreement with our findings from the TGA measurements of weight loss for the as-prepared and heat-treated LbL-PANi/MWNT films.

Figure 3 shows the Raman spectra of the LbL films along with the PANi nanofibers and MWNT as control. The functionalized MWNTs show two characteristic bands at 1580 cm^{-1} (G mode) for the phonon allowed high frequency mode and at 1355 cm^{-1} (D mode) for the disorder-induced peak due to the defects in rolled graphene sheets and tube ends due to COOH functionalization.[33] Similarly, all characteristic bands of PANi, such as C═C stretching of quinoid at 1580 cm^{-1}, C═N stretching of quinoid at 1486 cm^{-1}, and the aromatic C−H in-plane bending at 1166 cm^{-1}, can be observed for the PANi nanofibers.[34]

In Figure 3 (spectra c), the as-prepared LbL-PANi/MWNT film show characteristic Raman peaks at 1170 cm^{-1} for C−H bending of the quinoid ring, 1260 cm^{-1} for C−H bending of the benzoid ring, 1338 cm^{-1} for C−N^{*+} stretching for the radical cation, and 1484 cm^{-1} for the C═N stretching of the quinoid ring of PANi. Compared to the as-prepared LbL films, the heat-treated films show new bands at 1656 cm^{-1} that could be from the C═O or part of amide bonding between PANi and the MWNTs.

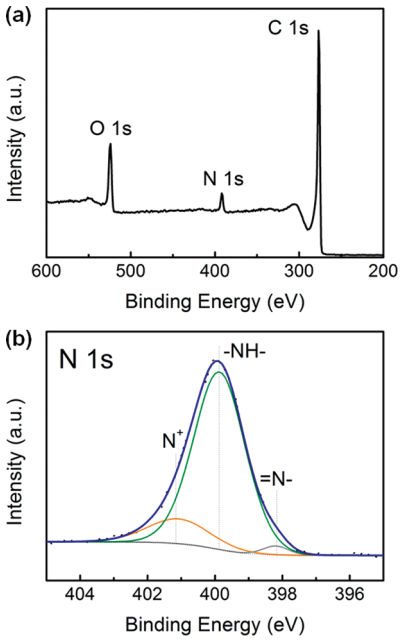

Figure 4. XPS spectra of the LbL-PANi/MWNT electrodes after heat treatment. (a) Survey scan, and (b) N 1s spectra.

The surface chemistry of LbL-PANi/MWNT electrodes after heat treatment was further investigated using X-ray photoelectron spectroscopy (XPS) spectra. A survey scan spectrum of LbL-PANi/MWNT films (Figure 4a) shows that a considerable amount of oxygen and nitrogen functional groups remained after heat treatment within the films. On the basis of high-resolution scan analysis of C, O, and N spectra, surface atomic composition of the films was found to be 86.8% carbon, 9.5% oxygen, and 3.7% nitrogen. An N 1s spectrum (Figure 4b) shows that the most nitrogen atoms are in the form of amine (-NH-) centered at 399.9 eV in benzenoid amine or amide groups.[35,36] Two small additional peaks suggest that some nitrogen atoms are imine groups (═NH-) centered at 398.2 eV and positively charged nitrogen groups (N^+) centered at 401.1 eV.[35]

Microstructure of LbL-PANi/MWNT Thin Films. Figure 5 shows tapping-mode AFM images of the LbL-PANi/MWNT thin films assembled with increasing numbers of bilayers. The AFM images clearly show that the LbL-PANi/MWNT thin films have an interconnected branched network structure with separated individual fibers and nanotubes. As can be seen in the inset of Figure 5a, the PANi nanofibers and MWNTs created highly entangled porous nanostructures where the root-mean-squared (rms) roughness increases with the number of bilayers. In Figure 5b, the increase in

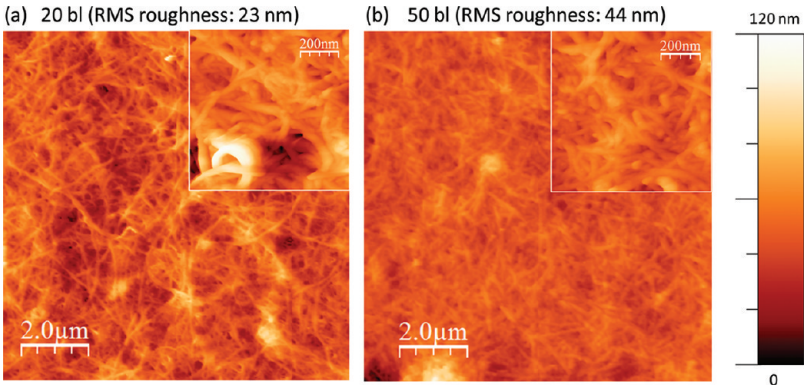

Figure 5. Atomic force microscopy (AFM) height images of LbL-PANi/MWNT thin films. Size of each image is 10 μm $\times$ 10 μm. (a) 20 bilayers, (b) 50 bilayers. Inset image sizes are 1 μm $\times$ 1 μm.

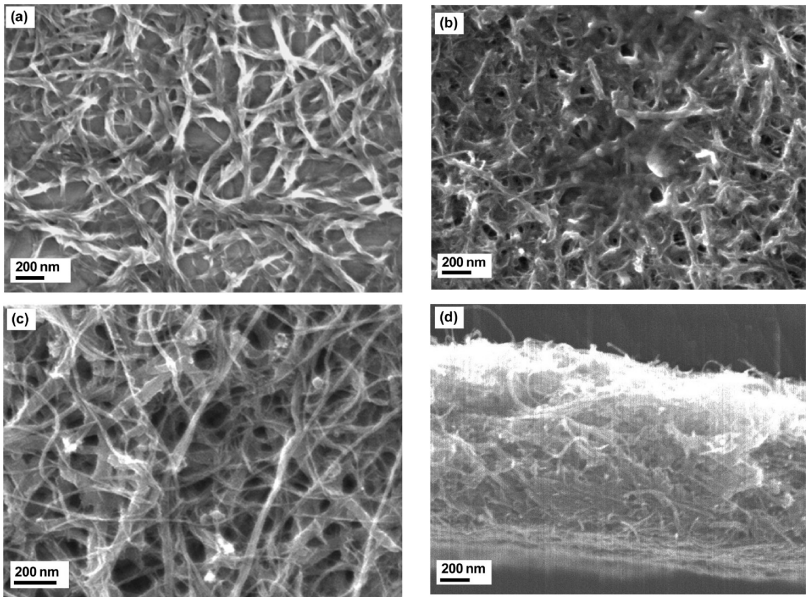

Figure 6. Scanning electron microscopy (SEM) images of (a) PANi nanofibers, (b) raw cast films of PANi and MWNT suspension, (c) LbL-PANi/MWNT film, and (d) cross-section view of the LbL film shown in panel c.

roughness can be explained by the higher thickness of the films with the number of bilayers and the film shows relatively uniform and somewhat more densely packed PANi and MWNT network structures.

Scanning electron microscopy (SEM) (Figure 6a) shows the microstructure of PANi nanofibers prepared from the rapid polymerization of aniline with ammonium peroxydisulfate in the presence of HCl. The PANi nanofibers (Figure 6a inset) do not have a uniform cylindrical or tubular structure, but rather they form a random, interconnected, nearly flat web structure of diameters roughly 30−70 nm and lengths 0.4−3 μm. This highly interconnected microstructure can act as an ideal support for the MWNT nanotubes. Figure 6b shows a raw cast film of PANi nanofibers and MWNT suspension (mixed solution was sonicated for 2 h) for comparison with the LbL films. The cast film shows aggregation and alignment of bundles of PANi nanofibers and MWNT due to ionic interaction, van der Waals interactions, and capillary forces. In addition, the cast film exhibits dense packing, poor stability, and poor control over thickness that lead to diminishment of the available surface area that were intrinsic to the PANi fibers and MWNTs, whereas in Figure 6c, the LbL assembled PANi/MWNT thin film shows an intertwined porous network structure of PANi nanofibers and MWNT nanotubes. Since the final layer of the LbL film was MWNT (polyanion), predominantly tubular MWNT is visible on top of the PANi nanofibers. Comparing Figure 6b and c, the assembled LbL films yield randomly oriented networks with well developed nanoscale pores. These highly nanoporous PANi/MWNT thin films could be ideal electrode materials with mixed ionic/electronic conducting channels. The electrostatic cross-linking between positively charged PANi nanofibers and negatively charged MWNTs during the LbL process leads to a randomly oriented, kinetically driven nanostructure. Figure 6d shows a cross-sectional view

of a PANi/MWNT thin film that demonstrates the conformal and uniform nature of the coating generated with LBL assembly of PANi nanofibers and MWNTs. The highly interpenetrated, nanoporous internal structure helps to achieve large surface area in the LbL films. This morphology could provide fast electronic and ionic conducting channels as the conjugate PANi nanofibers and MWNT nanotubes have intrinsically high surface area and electrical conductivity (0.8 S/cm for PANi nanofibers, 4.1 S/cm LbL-PANi/MWNT films).

TEM imaging was used to determine the detailed microstructure of PANi nanofibers and LbL-PANi/MWNT films. In Figure 7a, the PANi nanofiber morphology shows interconnected, branched, and networked structure. A representative TEM image of an LbL-PANi/MWNT film after heat treatment is shown in Figure 7b where a randomly oriented network structure can be seen. Figure 7c shows a magnified view of the PANi/MWNT film where a gray circle indicates one of the cross-linked points between PANi nanofiber and MWNTs within the network structure. It is clear that the MWNT in LbL films are not coated with the polymer (PANi), which is very common in polymer composites films where PANi and MWNT solution are simply mixed and the polymer creates a thin coating on individual nanotubes.[37] The layer-by-layer approach provides a unique way to fabricate nanostructured materials where the components can still retain their individual morphology but still provide improved physicochemical properties due to the cross-linked network.

Electrochemical Performance of LbL-PANi/MWNT Thin Film Electrodes. The energy storage mechanism of the LbL-PANi/MWNT films was investigated from cyclic voltammetry (CV) measurements in two-electrode lithium cells with 1 M $LiPF_6$ in a mixture of ethylene carbonate and dimethyl carbonate (v/v ratio 3:7) (Figure. 8). Figure 8a compares cyclic voltammograms of the LbL-PANi/MWNT film with that of the previously reported LbL-MWNT film.[3] The LbL-MWNT films showed high capacitance due to the utilization of Faradaic reactions between surface oxygen functional groups and lithium ions in lithium cells.[3] Volumetric currents of the LbL-PANi/MWNT film are much larger compared to those of the LbL-MWNT film in the voltage range from ~2.3 to 4.5 V *vs* Li, which results in higher volumetric capacitance (~238 ± 32 F/cm^3) of the LbL-PANi/MWNT compared to that of the LbL-MWNT electrodes (~180 F/cm^3). In addition, this volumetric capacitance (~238 ± 32 F/cm^3) in the lithium cell is comparable with ~248 ± 19 F/cm^3 achieved in a 1 M H_2SO_4 solution (−0.2 to 1.0 V *vs* Ag/AgCl) (Supporting Information, Figure S3), but utilizing about three times wider potential window compared to the aqueous system. Significant enhancement of volumetric capacitance of the LbL-PANi/MWNT films can be attributed to redox reactions of PANi, where oxidation states of PANi are changed by the doping/undoping

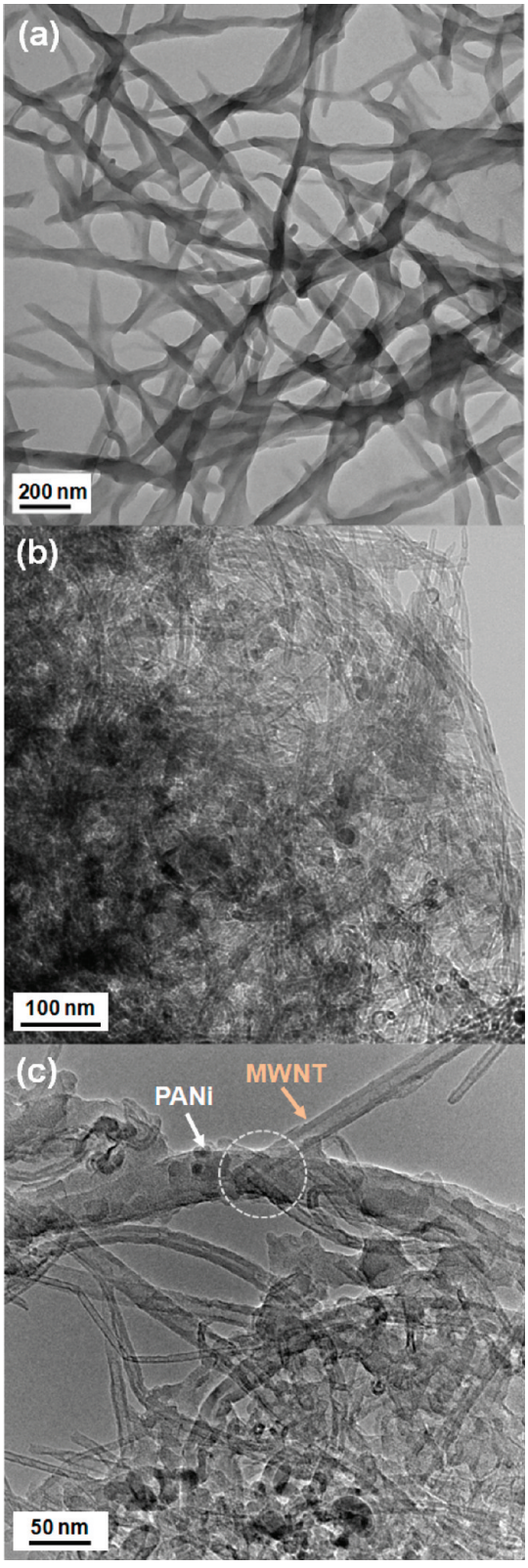

Figure 7. Transmission electron microscopy (TEM) images of (a) PANi nanofibers and (b, c) the LbL-PANi/MWNT films: (b) low-magnification and (c) high-magnification of LbL-PANi/MWNT electrodes after heat treatment (60 bilayers, 883 nm). White and orange arrows in panel c indicate PANi nanofiber and MWNT, respectively. Gray circle in panel c shows one of contact points between PANi nanofibers and MWNTS within the LbL-PANi/MWNT films.

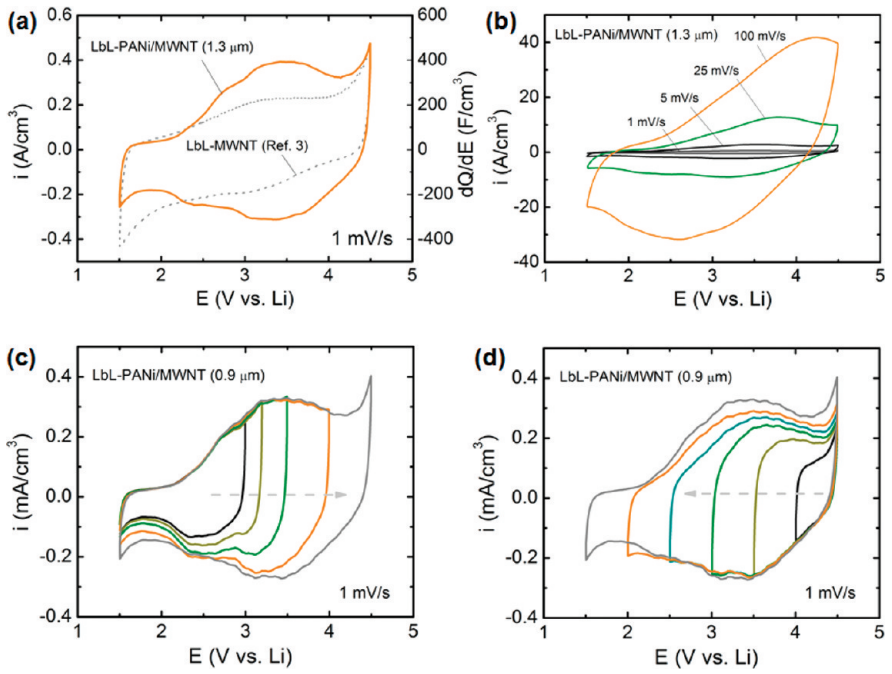

Figure 8. Cyclic voltammograms of LbL-PANi/MWNT electrodes after heat treatment in two-electrode lithium cells with 1 M $LiPF_6$ in a mixture of ethylene carbonate and dimethyl carbonate (v/v ratio 3:7) as the electrolyte. (a) Cyclic voltammogram comparison between the LbL-PANi/MWNT and the LbL-MWNT electrodes (ref 3). (b) Rate-dependent cyclic voltammograms of an LbL-PANi/MWNT electrode at various scan rates (1−100 mV/s). (c) Forward and (d) backward potential-dependent cyclic voltammograms of the LbL-PANi/MWNT electrodes.

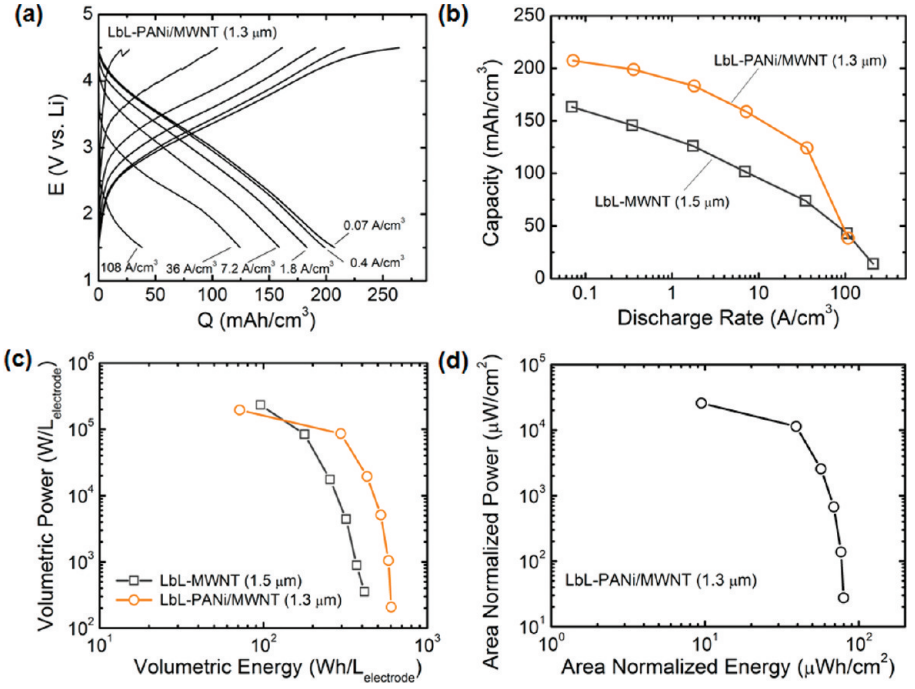

Figure 9. (a) Charge and discharge profiles of an LbL-PANi/MWNT electrode obtained over a wide range of volumetric current densities between 1.5 and 4.5 V *vs* Li. Before each charge and discharge measurement, cells were held at 1.5 and 4.5 V for 30−40 min. (b) Volumetric discharge capacity *vs* volumetric current and (c) Ragone plot (per electrode volume) comparison for the LbL-PANi/MWNT and the LbL-MWNT electrodes. (d) Electrode area normalized Ragone plot of the LbL-PANi/MWNT electrode.

of PF_6^- anions. Cyclic voltammograms of the LbL-PANi/MWNT films were also measured in 1 M $LiClO_4$ in propylene carbonate (PC), showing negligible differences in both shape and capacitance (Supporting Information, Figure S4). Figure 8b shows the rate-dependent cyclic voltammograms of the LbL-PANi/MWNT electrodes

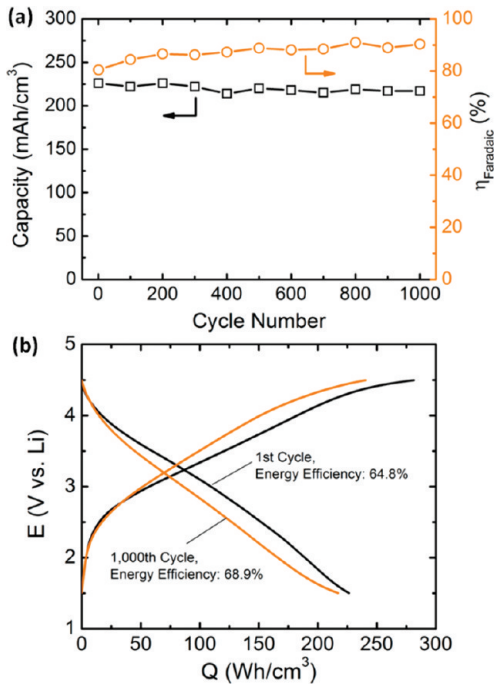

Figure 10. (a) Volumetric capacities of an LbL-PANi/MWNT electrode (0.9 μm) as a function of cycle number, measured at ~1 A/cm^3 once every 100 cycles, after holds at the end of charging and discharging for 30 min. Within each 100 cycles, these cells were cycled at an accelerated rate of ~100 A/cm^3. (b) Voltage profiles of the LbL-PANi/MWNT electrode in the first and 1,000th cycles, which include energy efficiency during the charge and discharge process.

over a wide range of scan rates, maintaining characteristic redox peaks of PANi up to 100 mV/s. Figure 8c and d show gradual increases in volumetric currents with increasing potential from 1.5 to 4.5 V *vs* Li and with decreasing potential from 4.5 to 1.5 V *vs* Li, respectively. These potential-dependent CV measurements clearly revealed the redox reaction processes of the LbL-PANi/MWNT electrodes at each potential.

Electrochemical performance of the LbL-PANi/MWNT electrodes was also investigated by rate-dependent galvanostatic measurements (Figure 9a). The LbL-PANi/MWNT electrode (1.3 μm thickness) shows a high volumetric capacity of ~210 mAh/cm^3 at low discharge rate (0.07 A/cm^3) and maintained ~75% of capacity (160 mAh/cm^3) at ~7.2 A/cm^3. Figure 9b compares volumetric capacities of the LbL-thin film electrodes as a function of discharge rates, showing much higher volumetric capacities of the LbL-PANi/MWNT compared to the LbL-MWNT electrodes until ~100 A/cm^3. Corresponding Ragone plots (Figure 9c) based on the volume of LbL-films show that the LbL-PANi/MWNT films can deliver much higher energy than LbL-MWNT films below 100 kW/$L_{electrode}$. It is interesting that the LbL-MWNT films can deliver a high energy density in the extremely high power region (>100 kW/$L_{electrode}$) compared to the LbL-PANi/MWNT films; this can be attributed to the high electrical conductivity of the LbL-MWNT (~10 S/cm) compared to that of the

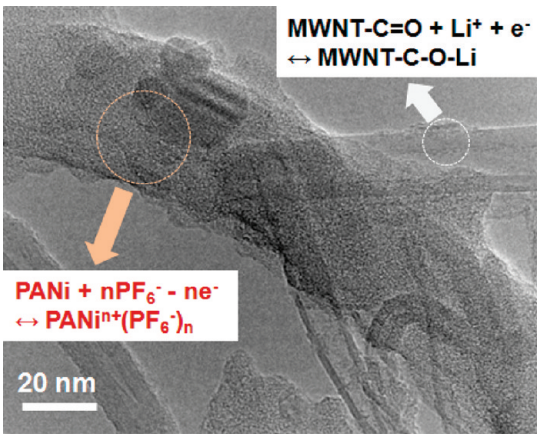

Figure 11. (a) Schematic of the energy storage mechanism on a TEM image of the LbL-PANi/MWNT electrode. The white circle indicates surface functional groups on MWNTs, and the orange circle indicates the surface of PANi.

LbL-PANi/MWNT electrodes (~4.1 S/cm). The LbL-PANi/MWNT electrode can deliver ~500 Wh/$L_{electrode}$ in the lower power region of ~5 kW/$L_{electrode}$, and maintain ~220 Wh/$L_{electrode}$ in the high power region of ~100 kW/$L_{electrode}$. The corresponding gravimetric energy and power density of the LbL-PANi/MWNT electrodes were converted by dividing by the density of the film (0.57 g/cm^3) as shown in Supporting Information, Figure S5, showing ~1 kWh/$kg_{electrode}$ at ~1 kW/$kg_{electrode}$. For thin film microbatteries it is convenient to compare geometric area normalized energy and power density since this comparison does not depend on the choice of other components including substrates and protective packaging.[1] Representative area normalized energy and power densities of the LbL-PANi/MWNT thin films are ~75 μWh/cm^2 in the low power region of ~100 μW/cm^2 and ~40 μWh/cm^2 in the high power region of ~10 mW/cm^2. Moreover, LbL-PANi/MWNT electrodes show good cycle stability up to 1,000 cycles with only 4% decay in capacity, as shown in Figure 10a. It is interesting to note that Faradaic efficiency gradually increases from ~80% in the first cycle to ~90% after 1,000 cycles. However, it should be mentioned that a limitation of LbL-PANi/MWNT films in lithium cells is the low energy efficiency of ~65% due to large polarization during the charge and discharge cycles (Figure 10b).

CONCLUSIONS

Novel LbL-PANi/MWNT thin film electrodes have been successfully prepared with positively charged acid doped PANi and negatively charged carboxylic acid functionalized MWNT using layer-by-layer self-assembly. The surface charge density of PANi nanofibers and MWNT allows excellent control of film thickness and roughness by adjusting the charge reversal mechanism and interpenetration. The heat-treated LbL-PANi/MWNT thin films show a cross-linked reticulated

structure with well-defined nanopores and interconnectivity, which can facilitate fast electron and ion transport. The LbL-PANi/MWNT electrodes can exhibit both high energy and high power density (~220 Wh/$L_{electrode}$ at ~100 kW/$L_{electrode}$) with long cycle life in a lithium cell. Faradaic reactions between PANi fiber and PF_6^- anions as well as redox reactions between oxygen functional groups on MWNTs and lithium ions in lithium cells are the origin of the high energy density of the electrodes, as can be seen schematically in the high-resolution TEM image in Figure 11. In addition, high values of the area normalized energy and power density of the LbL electrode indicate the potential to gain precise control of energy and power storage of thin film microbatteries by controlling the number of bilayers and film thickness in the LbL assembly. Finally, the integration of the LbL films on various substrates including Si wafers, glass, and flexible substrates can be a promising strategy to design next generation microbatteries or ECs for portable electronic devices, microelectromechanical systems (MEMS), sensors, and actuator devices.

METHODS

Layer-by-Layer Assembly of PANi/MWNT Thin Films. PANi nanofibers were prepared by rapid polymerization[9] of aniline (99.5% purity) with ammonium peroxydisulfate (99% purity). Briefly, aniline hydrochloride (purum; 2.59 g, 20 mmol) was dissolved in distilled 1 M HCl in a volumetric flask to 50 mL of solution. Ammonium peroxydisulfate (purum; 5.71 g, 25 mmol) was dissolved in 1 M HCl also to 50 mL of solution. Both solutions were kept for 1 h at room temperature (~18−24 °C), then mixed in a beaker, briefly stirred, and left at rest to polymerize for 24 h. Then the PANi was collected as a fiber suspension using a centrifuge (at 10,000 rpm for 15 min) after being washed two times with 100 mL of deionized Milli-Q water adjusted to pH ~2.5, and the fibers were resuspended. MWNTs were purchased from NANOLAB (95% purity, length 1−5 μm, outer diameter 15 ± 5 nm) and were modified by carboxylic acid functionalization (MWNT-COOH) described elsewhere.[23] Suspensions of PANi fibers and MWNT nanotubes were sonicated using a Branson Bransonic 3510 ultrasonic cleaner (40 kHz) in Milli-Q water (18.2 MΩ·cm) for 15 min to form stable dispersions. These suspensions were subjected to dialysis against Milli-Q water for several days to remove any byproduct or residual material from polymerization or functionalization. The concentrations (0.5 mg/mL) and pH levels of the solutions were precisely adjusted after dialysis, and the resulting suspensions were sonicated briefly prior to LbL assembly (Scheme 1). PANi/MWNT films were fabricated with a StratoSequence VI automated dipping robot with rotating sample holder (nanoStrata, Inc.) on various substrates such as ITO slides, glass slides, and silicon wafers. The dipping time in each polyelectrolyte solution was 15 min followed by three rinse baths of Milli-Q water for 3, 1, and 1 min each, respectively. This cycle makes one bilayer (bL) of PANi and MWNT, denoted (LbL-PANi/MWNT). The cycle was repeated to reach the desired number of bilayers of LbL-PANi/MWNT thin films. To enhance the adhesion and stability of the LbL films on various substrate (ITO, glass slides), prior to the application of PANi and MWNT polyelectrolytes, base layers (2 bL assembled at pH ~4.0) of linear polyethylenimine (LPEI, 25,000 M_w, monodispersed, Polysciences) and poly(acrylic acid) (PAA, 90,000 M_w, polydispersity index (PDI) 4, 25% aqueous solution, Polysciences) were used as received and prepared as 20 mM solutions in deionized water, based on the repeat-unit molecular weight. The as-prepared PANi/MWNT films were heat-treated at 180 °C for 12 h in vacuum to improve the stability of the films. Any LbL-PANi/MWNT films over 30 bilayers were heat-treated more than once to control the interdiffusion, *e.g.*, LbL-$(PANi/MWNT)_{50}$ film was heat-treated twice, once after the first 30th bilayer and then after the 50th bilayer during LbL assembly.

Characterization. The zeta potential of PANi and MWNT as a function of pH was measured using a Zeta PALS instrument (Brookhaven Instrument Corp.) to determine the effect of surface charge on PANi nanofibers and MWNTs dispersions. Thickness of PANi/MWNT thin films on glass slides was determined using a Veeco Dektak 150 profilometer. Surface topology of PANi/MWNT thin films was examined using an AFM microscope (Veeco Dimension 3100) in the tapping mode in air. The root-mean-square (rms) roughness of the LbL films was examined from AFM images with a size of 6 μm × 6 μm. Surface morphology and interior structure of PANi/MWNT LbL films were investigated using a scanning electron microscope (JEOL 6320FV Field-Emission High-Resolution SEM) operating at 3.0 and 5.0 kV and a transmission electron microscope (JEOL 2010/2010F Advanced High Performance TEM) for medium and high resolution imaging. The surface chemistry of PANi nanofibers, functionalized MWNTs, and the LbL-PANi/MWNT films were analyzed using a Raman Spectrometer (Kaiser Hololab 5000R) operating at 785 nm utilizing Coherent CW argon/ion and Ti/S lasers and a Kratos AXIS Ultra Imaging X-ray photoelectron spectrometer (XPS). The N 1s peak was calibrated with the C 1s photoemission peak for sp^2-hybridized carbon centered at 284.5 eV. Thermal behavior of the LbL films were analyzed with a thermogravimetric analyzer (TA Instruments Q50) in air/N_2 at a heating rate of 10 °C/min. Sheet resistances were measured for films deposited on glass slides by using a standard four-point probe configuration (Keithley SCS-4200). A series of 3or 4 measurements were taken on each film, and the measurements then were averaged to give the final reported value with the standard deviation as an error range.

Electrochemical Measurement of LbL-PANi/MWNT Electrodes. A three-electrode cell was employed for electrochemical measurements in the aqueous-cell test, where a Ag/AgCl electrode (BASi) (3 M NaCl) and Pt wire were used as the reference and counter electrodes, respectively. LbL-PANi/MWNT films on ITO-coated glass slides were used as the working electrode. Cyclic voltammetry was performed between −0.2 and 1.0 V (Ag/AgCl) at room temperature in 1 M H_2SO_4 solution using a bipotentiostat (PINE instrument). The lithium-cell test was conducted using a two-electrode electrochemical cell (Tomcell Co. Ltd.) consisting of LbL-PANi/MWNT films on ITO-coated glass slides as the positive electrodes and lithium foils as the negative electrodes. A piece of aluminum foil was attached to one side of the ITO-coated glass slide and used as a current collector. The electrolyte solutions were 1 M $LiPF_6$ in ethylene carbonate (EC) and dimethyl carbonate (DMC) 3:7 vol % (Kishida Chem. Corp. Ltd.) contained within two Celgard 2500 microporous separators and 1 M $LiClO_4$ in propylene carbonate (PC) (also from Kishida Chem. Corp. Ltd., Japan) contained within two Celgard 3501 separators. The electrode area of LbL-PANi/MWNT electrodes was 1.05 cm^2, and the loading density was 0.15−0.23 mg/cm^2. Li-cell testing was performed using a Solartron 4170 in the voltage range 1.5−4.5 V *vs* Li at room temperature.

Acknowledgment. The authors acknowledge Contour Energy for funding support of this project. This work made use of the Shared Experimental Facilities supported by the MRSEC Program of the National Science Foundation under award number DMR 02-13282. M.N.H. acknowledges the support of a postdoctoral fellowship from the Natural Sciences and Engineering Research Council (NSERC) of Canada. S.W.L.

acknowledges a Samsung Scholarship from the Samsung Foundation of Culture.

Supporting Information Available: Additional figures as described in the text. This material is available free of charge *via* the Internet at http://pubs.acs.org.

REFERENCES AND NOTES

1. Dudney, J. N. Thin Film Micro-batteries. *Electrochem. Soc. Interface* **2008**, *17*, 44–48.
2. Simon, P.; Gogotsi, Y. Materials for Electrochemical Capacitors. *Nat. Mater.* **2008**, *7*, 845–854.
3. Lee, S. W.; Yabuuchi, N.; Gallant, B. M.; Chen, S.; Kim, B. S.; Hammond, P. T.; Shao-Horn, Y. High-power Lithium Batteries from Functionalized Carbon-Nanotube Electrodes. *Nat. Nanotechnol.* **2010**, *5*, 531–537.
4. Pech, D.; Brunet, M.; Durou, H.; Huang, P. H.; Mochalin, V.; Gogotsi, Y.; Taberna, P. L.; Simon, P. Ultrahigh-Power Micrometre-Sized Supercapacitors based on Onion-like Carbon. *Nat. Nanotechnol.* **2010**, *5*, 651–654.
5. Arico, A. S.; Bruce, P.; Scrosati, B.; Tarascon, J. M.; Van Schalkwijk, W. Nanostructured Materials for Advanced Energy Conversion and Storage Devices. *Nat. Mater.* **2005**, *4*, 366–377.
6. Lee, S. W.; Gallant, B. M.; Byon, H. R.; Hammond, P. T.; Shao-Horn, Y. Nanostructured Carbon-Based Electrodes: Bridging the Gap Between Thin-Film Lithium-Ion Batteries and Electrochemical Capacitors. *Energy Environ. Sci.* **2011**, *4*, 1972–1985.
7. Hu, L. B.; Wu, H.; La Mantia, F.; Yang, Y. A.; Cui, Y. Thin, Flexible Secondary Li-Ion Paper Batteries. *ACS Nano* **2010**, *4*, 5843–5848.
8. Macdiarmid, A. G.; Chiang, J. C.; Richter, A. F.; Epstein, A. J. Polyanine—A New Concept in Conducting Polymers. *Synth. Met.* **1987**, *18*, 285–290.
9. Huang, J. X.; Kaner, R. B. A General Chemical Route to Polyaniline Nanofibers. *J. Am. Chem. Soc.* **2004**, *126*, 851–855.
10. Long, Y. Z.; Chen, Z. J.; Zhang, X. T.; Zhang, J.; Liu, Z. F. Synthesis and Electrical Properties of Carbon Nanotube Polyaniline Composites. *Appl. Phys. Lett.* **2004**, *85*, 1796–1798.
11. Wu, M. Q.; Zhang, L. P.; Wang, D. M.; Gao, J. H.; Zhang, S. R. Electrochemical Capacitance of MWCNT/Polyaniline Composite Coatings Grown in Acidic MWCNT Suspensions by Microwave-assisted Hydrothermal Digestion. *Nanotechnology* **2007**, *7*, 385603–385610.
12. Meng, C. Z.; Liu, C. H.; Fan, S. S. Flexible Carbon Nanotube/Polyaniline Paper-like Films and Their Enhanced Electrochemical Properties. *Electrochem. Commun.* **2009**, *11*, 186–189.
13. Tran, H. D.; Li, D.; Kaner, R. B. One-Dimensional Conducting Polymer Nanostructures: Bulk Synthesis and Applications. *Adv. Mater.* **2009**, *21*, 1487–1499.
14. Iijima, S. Helical Microtubules of Graphitic Carbon. *Nature* **1991**, *354*, 56–58.
15. Jain, V.; Yochum, H. M.; Montazami, R.; Heflin, J. R.; Hu, L. B.; Gruner, G. Modification of Single-Walled Carbon Nanotube Electrodes by Layer-by-Layer Assembly for Electrochromic Devices. *J. Appl. Phys.* **2008**, 103.
16. Lota, G.; Fic, K.; Frackowiak, E. Carbon Nanotubes and Their Composites in Electrochemical Applications. *Energy Environ. Sci.* **2011**, *4*, 1592–1605.
17. Pan, L. J.; Pu, L.; Shi, Y.; Song, S. Y.; Xu, Z.; Zhang, R.; Zheng, Y. D. Synthesis of Polyaniline Nanotubes with a Reactive Template of Manganese Oxide. *Adv. Mater.* **2007**, *19*, 461–464.
18. Li, W. G.; McCarthy, P. A.; Liu, D. G.; Huang, J. Y.; Yang, S. C.; Wang, H. L. Toward Understanding and Optimizing the Template-guided Synthesis of Chiral Polyaniline Nanocomposites. *Macromolecules* **2002**, *35*, 9975–9982.
19. Huang, J. X. Syntheses and Applications of Conducting Polymer Polyaniline Nanofibers. *Pure Appl. Chem.* **2006**, *78*, 15–27.
20. Decher, G. Fuzzy Nanoassemblies: Toward Layered Polymeric Multicomposites. *Science* **1997**, *277*, 1232–1237.
21. Zhang, M. N.; Yan, Y. M.; Gong, K. P.; Mao, L. Q.; Guo, Z. X.; Chen, Y. Electrostatic Layer-by-Layer Assembled Carbon Nanotube Multilayer Film and Its Electrocatalytic Activity for O_2 Reduction. *Langmuir* **2004**, *20*, 8781–8785.
22. Zhang, M. N.; Su, L.; Mao, L. Q. Surfactant Functionalization of Carbon Nanotubes (CNTs) for Layer-by-Layer Assembling of CNT Multi-layer Films and Fabrication of Gold Nanoparticle/CNT Nanohybrid. *Carbon* **2006**, *44*, 276–283.
23. Lee, S. W.; Kim, B. S.; Chen, S.; Shao-Horn, Y.; Hammond, P. T. Layer-by-Layer Assembly of All Carbon Nanotube Ultrathin Films for Electrochemical Applications. *J. Am. Chem. Soc.* **2009**, *131*, 671–679.
24. Olek, M.; Ostrander, J.; Jurga, S.; Mohwald, H.; Kotov, N.; Kempa, K.; Giersig, M. Layer-by-Layer Assembled Composites from Multiwall Carbon Nanotubes with Different Morphologies. *Nano Lett.* **2004**, *4*, 1889–1895.
25. Chen, J.; Hamon, M. A.; Hu, H.; Chen, Y. S.; Rao, A. M.; Eklund, P. C.; Haddon, R. C. Solution Properties of Single-Walled Carbon Nanotubes. *Science* **1998**, *282*, 95–98.
26. Choi, J.; Rubner, M. F. Influence of the Degree of Ionization on Weak Polyelectrolyte Multilayer Assembly. *Macromolecules* **2005**, *38*, 116–124.
27. Porcel, C.; Lavalle, P.; Decher, G.; Senger, B.; Voegel, J. C.; Schaaf, P. Influence of the Polyelectrolyte Molecular Weight on Exponentially Growing Multilayer Films in the Linear Regime. *Langmuir* **2007**, *23*, 1898–1904.
28. Zacharia, N. S.; DeLongchamp, D. M.; Modestino, M.; Hammond, P. T. Controlling Diffusion and Exchange in Layer-by-Layer Assemblies. *Macromolecules* **2007**, *40*, 1598–1603.
29. Zacharia, N. S.; Modestino, M.; Hammond, P. T. Factors Influencing the Interdiffusion of Weak Polycations in Multilayers. *Macromolecules* **2007**, *40*, 9523–9528.
30. Yoo, P. J.; Zacharia, N. S.; Doh, J.; Nam, K. T.; Belcher, A. M.; Hammond, P. T. Controlling Surface Mobility in Interdiflusing Polyelectrolyte Multilayers. *ACS Nano* **2008**, *2*, 561–571.
31. Ansari, R.; Wallace, G. G. Effect Of Thermal-Treatment On the Electrochemical Properties of Conducting Polypyrrole Polymers. *Polymer* **1994**, *35*, 2372–2377.
32. Lu, J. B.; Park, B. J.; Kumar, B.; Castro, M.; Choi, H. J.; Feller, J. F. Polyaniline Nanoparticle-Carbon Nanotube Hybrid Network Vapour Sensors with Switchable Chemo-electrical Polarity. *Nanotechnology* **2010**, *21*, 255501–255511.
33. Arsov, L. D.; Plieth, W.; Kossmehl, G. Electrochemical and Raman Spectroscopic Study of Polyaniline; Influence of the Potential on the Degradation of Polyaniline. *J. Solid State Electr.* **1998**, *2*, 355–361.
34. Wang, X. C.; Li, Y.; Zhao, Y.; Liu, J.; Tang, S. D.; Feng, W. Synthesis of PANI Nanostructures with Various Morphologies from Fibers to Micromats to Disks Doped with Salicylic Acid. *Synth. Met.* **2010**, *160*, 2008–2014.
35. Kang, E. T.; Neoh, K. G.; Tan, K. L. Polyaniline: A Polymer with Many Interesting Intrinsic Redox States. *Prog. Polym. Sci.* **1998**, *23*, 277–324.
36. Harris, J. J.; DeRose, P. M.; Bruening, M. L. Synthesis of Passivating, Nylon-like Coatings through Cross-linking of Ultrathin Polyelectrolyte Films. *J. Am. Chem. Soc.* **1999**, *121*, 1978–1979.
37. Wu, T. M.; Lin, Y. W. Doped Polyaniline/Multi-walled Carbon Nanotube Composites: Preparation, Characterization and Properties. *Polymer* **2006**, *47*, 3576–3582.